HARMONIA
International network for harmonization of atmospheric aerosol retrievals from ground based photometers

HARMONIA CA21119

Deliverable 2.3

a. Report on the links of metrology MAPP project results and measurement accuracy and uncertainty improvements
b. an example of machine learning techniques towards the retrieval of aerosol properties

Authors

a. S. Kazadzis[1], V. Estelles[2] M. Campanelli[3]

Using material from publications of
N. Kouremeti et. al., J. Gröbner et al., J. Elsey et al.
And MAPP project reports

b. F. Scarlatti[2]

Based on: "Aerosol properties retrieval in partially cloud conditions using HDR All-Sky imagery" presentation at European Meteorological Symposium, 2024.

1. Physikalisch-Meteorologisches Observatorium Davos, World Radiation Center, Switzerland
Earth Physics and Thermodynamics Department,
2. Universitat de València, Valencia, 46100, Spain
3. Institute of Atmospheric Sciences and Climate (ISAC), Consiglio Nazionale Delle Ricerche (CNR), Rome, 00133, Italy

Date 11 October 2024

a. Report on the links of the project Metrology of Aerosol Optical Properties metrology (MAPP) results and Harmonia objectives on calibration and uncertainty

Motivation

The Metrology of Aerosol Optical properties (MAPP) was a Metrology (EMPIR) funded project (06.2020 - 05.2023). One of the basic aims of MAPP was to enable the SI-traceable measurement of column-integrated aerosol optical properties retrieved from the passive remote sensing of the atmosphere using solar and lunar radiation measurements. The main goal was to standardize aerosol optical properties retrieval by shortening the calibration chain, reduce calibration downtime of network radiometers and establish their consistent dissemination including their uncertainty. Aspects directly linked with objectives of the first 2 Harmonia workpackages.

More specific one of the four main objectives of the project was: "*To develop a comprehensive uncertainty budget for aerosol optical properties, such as aerosol optical depth, aerosol size distribution, and aerosol single scatter albedo, retrieved from remote sensing-based measurements of direct and scattered solar radiation, enabling its inclusion in the corresponding data archives of the aerosol monitoring networks, with the relevant calibration and traceability information.*"

Main objective of this report is to summarize the MAPP findings related to HARMONIA and disseminate them into the Harmonia Community through the related deliverable. The report includes the motivation, highlights and main conclusions from three publications that came as an outcome of MAPP and in addition an uncertainty analysis overview for sun photometers, reported in MAPP.

Introduction

Atmospheric aerosols are minor constituents of the atmosphere but an important component in terms of impacts on the climate. Based on the main global

Atmospheric Watch program of the World Meteorological Organization, long term monitoring of aerosol essential climate variables (ECVs) including their uncertainties is needed for observing sensitive changes in the Earth climate system. Aerosol optical properties from ground-based passive remote sensing radiometers have been retrieved consistently for the past 25-30 years.

Currently, aerosol optical remote sensing networks rely either on a calibration hierarchy, based on bilateral comparisons between network and reference instruments (e.g. AERONET, GAWPFR), or on in situ calibrations (SKYNET) of network radiometers, **without any link to traceable standards**. The crucial element in this process is knowledge of the irradiance at the top of atmosphere (ToA), solar or lunar. The state of the art established methodology for obtaining the ToA spectral irradiances is through in situ calibrations of the reference radiometers based on zero-air-mass extrapolations (also called Langley-plot procedures) at pristine high-altitude sites (Shaw, 1983; Toledano et al., 2018, and references therein). Then, assuming absolute stability of the radiometers, these are relocated to their respective calibration sites (for example Physikalisch-Meteorologisches Observatorium Davos, World Radiation Center – PMOD/WRC, Davos, Switzerland, for GAW-PFR or Observatoire de Haute-Provence, France, and Valladolid and Izaña, Spain, in the case of AERONET Europe) to transfer their ToA irradiance values to the network radiometers.

In a more rigorous approach, the AOD retrieval would involve SI-traceable solar irradiance measurements from ground-based filter-radiometers or spectroradiometers combined with calibrated and validated high spectral resolution TOA solar spectra (absolutely calibrated too), thereby circumventing the need for the subjective Langley-based calibration process.

In this report we aim to provide a summary of scientific publications, reports and scientific presentations within the MAPP project with emphasis on the calibration and AOD uncertainty aspects that are directly linked with the relevant objectives of Harmonia.

More specific we aim to provide the following chapters based on the above-mentioned publications and reports:

- An overview of the uncertainty estimation for AOD measurements
- SI-traceable solar irradiance measurements for aerosol optical depth retrieval using multifilter radiometers
- Spectral aerosol optical depth from SI-traceable spectral solar irradiance measurements

- Sensitivity of global direct aerosol radiative forcing to uncertainties in aerosol optical properties

An overview of the uncertainty estimation for AOD measurements (Langley or in situ calibration)

The spectral AOD is calculated using the Beer-Lambert law as,

$$\tau_{aod} = \left[log\left(\frac{Ic}{Io}\right) + \left(\tau_{ray} m_{ray} + \sum_i \tau_i m_i\right)\right]/m \qquad (1)$$

Where the wavelength term has been omitted for simplicity.

Expanded to explicitly mention all main gases, yields the measurement equation for AOD,

$$\tau_{aod} = \left[log(I) - log\,(I_0) + \left(XS_{ray} m_{ray}\, {}^{P}/_{P_0} + \tau_{NO2} m_{NO2} + \tau_{O3} m_{O3} + \tau_{H2O} m_{H2O} + \tau_{CO2,CH4} m_{CO2,CH4}\right)\right]/m$$

Where $\tau_{TraceGas} = TC_{TraceGas}\, XS_{TraceGas}$

Where the wavelength term has been omitted for simplicity.

Ic is the measured direct solar irradiance I (signal or calibrated) corrected for the contributions of cleaning efficiency $I^{rel}_{Cleaning}$, straylight in the FOV of the instrument $I^{rel}_{FOV_{strl}}$ and attenuation due to clouds I^{rel}_{Clouds}., I_0 is the solar irradiance at the top of the atmosphere, τ_{ray} is the optical depth of Rayleigh scattering, m_{ray} is the airmass for Rayleigh scattering, τ_{NO2} is the optical depth of nitrogen dioxide, m_{NO2} is the airmass for nitrogen dioxide, τ_{O3} is the ozone optical depth, τ_{H2O} is the optical depth of water vapor, corrected at 1020 nm and 1640 nm (CIMEL radiometer), $\tau_{CO2,CH4}$ is the optical depth of CO2-CH4, corrected at 1640 nm (CIMEL radiometer), m_{H2O} is the airmass for water vapor, $m_{CO2\text{-}CH4}$ is the airmass for CO2-CH4, m_{O3} is the ozone airmass, m is the aerosol airmass, P is the pressure at the site, P0 is the pressure at 1 atm, 1013.25 mbar, $TC_{TraceGas}$ total column of trace gas, $XS_{TraceGas}$ trace gas absorption cross-section weighted by the normalized measured or assumed responsivity of the filter with centroid wavelength λ

Here we present as an example the uncertainty analysis of AOD measurements with a Precision Filter Radiometer (PFR) as reported in the MAPP project:

The uncertainty budget is calculated from the individual uncertainty components according to

$$u = \sqrt{\sum_i \left(\left(\frac{\partial f}{\partial x_i} \right) \cdot u_{xi} \right)^2}$$

The partial derivatives for u_{xi} for different components included in the Beer-Lambert equation.

Direct solar irradiance measurement

The measurement uncertainty u_i is composed of the uncertainty of the data acquisition unit u_{daq}, the uncertainty in the dark signal, u_{dark}, the standard deviation of the measurements, u_{std}, the electronic stability of the instrument and the DAQ system u_{ref} 2.5V and the uncertainty $u_{FOV\text{-}Hom}$ associated with the pointing tolerance of 10 arcmin from the centre of the plateau in conjunction with the field of view homogeneity of 2%.
The relative standard measurement uncertainty u_I is:

$$u_I = \sqrt{\left[\frac{u_{daq}}{S}\right]^2 + \left[\frac{u_{dark}}{S}\right]^2 + \left[\frac{u_{std}}{100\sqrt{N}}\right]^2 + \left[\frac{u_{FOV-Hom}}{100}\right]^2}$$

Top of atmosphere solar irradiance

The ToA irradiance value is retrieved by the Langley extrapolation procedure of several days of measurements. PFR Langley are performed in a 6-month period. This aims in increasing the number of Langley days in the statistics, based on the fact that instruments have negligible change in responsivity within this period. The average number of points used is in the order of 70. Based on Eq. 1 the AOD uncertainty, that is related only to the Langley calibration factor I_0 ,equals $\frac{u_{ln(I_0)}}{m}$ where $u_{ln(I_0)}$is the uncertainty of Napierian logarithm of I_0 defined be the Langley extrapolation or the relative uncertainty of I_0, $u_{ln(I_0)} = \frac{a u_{I0}}{I_0} = u_{I0}$.

The uncertainty of $ln(I_0)$ can be described by the coefficient of variation (standard deviation / mean, (CV)) or in the case of a normal distribution by the standard error (standard deviation divided by the square root of the number of measurements, (SE)) .

Rayleigh optical depth

The Rayleigh optical depth is calculated according to the formula of Bodhaine, 1999, or Nicolet, 1984. For the wavelength range between 300 nm and 1200 nm and at STP,

the Rayleigh optical depth calculated with the two formulas, diverge by not more 0.001 in optical depth. Therefore, the standard uncertainty $u_{ray} = 0.001/\sqrt{3} = 5.8 * 10^{-4}$.

Ambient pressure

The ambient pressure is monitored with a calibrated air pressure sensor connected to the data acquisition system of the PFR unit. The corresponding standard uncertainty u_P is assumed to be less than 2 mbar. The main impact is on the Rayleigh correction, so at 500 nm, and using the formula of Bodhaine, the sensitivity coefficient $\frac{\vartheta \tau_{aod}}{\vartheta P}$ $can\ be\ assumed\ equal\ to$ $1.4 * 10^{-4} \frac{1}{m}$

Ozone optical depth

The only sensitivity to atmospheric ozone for PFR wavelengths is for the 500 nm channel of the PFR. For all other channels it is assumed to be negligible. The uncertainty of the total column ozone is assumed to be maximal 10 DU (uncertainty of the climatology used), which at 500 nm and using the absorption ozone cross-sections of Serdyuchenko et al., 2013 at -45 °C results in a standard expanded uncertainty of $u_{O3} = \frac{3.16e^{-4}}{\sqrt{3}} = 6 * 10^{-5}$

Nitrogen Dioxide optical depth

The sensitivity to nitrogen dioxide is calculated similarly to the one for atmospheric ozone. Use of climatological NO2 values can lead to related uncertainties especially in urban areas. No NO2 correction leads to a systematic overestimation of the calculated AOD, which is negligible for pristine conditions related stations.

Airmass calculation

Uncertainty in the optical path for aerosols (m) is calculated assuming the aerosol layer at 4 km and an uncertainty of ±1 km of the layer height.

$u_m = \Delta m/\sqrt{3}$ = 0.001/$\sqrt{3}$)= 5.7735e-04.

In the case of ozone airmass, the height of the effective ozone layer is assumed to be at 22 km. The seasonal variability of this height depends on latitude and can be up to 4 km at low to middle latitudes. The corresponding uncertainty of the airmass calculation

$u_{mO3} = \Delta m_{O3}/\sqrt{3}$ = 0.003/$\sqrt{3}$)= 0. 0017

For NO2 airmass, the height of the peak concentration of NO_2 is assumed to be at the same height of the aerosol layer.

$u_{mNO2} = u_m$

Field of view stray light

The stray light from the finite field of view depends strongly on the amount and type of aerosols, which affects the forward scattering into the field of view of the instrument. For reference instruments and pristine conditions, the uncertainty is less than 0.5% of the measured AOD for all wavelengths.

Instruments performing measurements at areas with large particles (e.g. Deserts) would have additional uncertainties due to the larger effect of forward scattering. For that case we have calculated using two conditions/scenarios: AOD at 500 nm [0.15 0.4] (global average and relatively high) and two aerosol mean effective radii [0.2 1.5] (μm) (small and large particles). The forward scattered radiation is also a function of the airmass, with larger scattering at higher airmass (Cuevas et al., 2019)

Window cleaning

For daily cleaning, the differences are less than 0.1% in signal levels.

Cloud contamination

The uncertainty described here is for best case scenarios for clear sky conditions. For this report, it is assumed to be zero. It is a difficult parameter to assess. For a network product it is non-zero, but for a reference measurement it can be assumed zero (best case conditions).

Full Uncertainty Budget for PFR-CIMEL-POM Prede is presented in Annex 1.

SI-traceable solar irradiance measurements for aerosol optical depth retrieval using multifilter radiometers

The overall aim of the study Kouremeti et al., 2023, is to enable the traceability? to International System of Units (SI) determination of column-integrated aerosol optical depth (AOD) retrieved from the passive remote sensing of the atmosphere. A PFR instrument has been characterized and calibrated at the state-of-the-art calibration facilities of Physikalisch-Technische Bundesanstalt (PTB). The measured SI-traceable solar irradiances together with three state-of-the-art ToA solar spectra have been used for retrieving AODs. These were validated against the reference AOD instruments of the World Aerosol Optical Depth Calibration Centre of the World Meteorological Organization (WMO).

Measurement set up at the PTB

PFR-N-001 was characterized and calibrated at PTB in November 2018 and once again in January 2021. The characterization and calibration in 2018 were performed using a setup based on a ns-pulsed optical parametric oscillator (OPO) system (EKSPLA NT242) and the tunable lasers in photometry (TULIP) setup based on a fs-OPO system (Schuster *et al* 2014). There, the spectral irradiance responsivities of the four channels were measured within the respective in-band spectral ranges. The wavelength was measured by an array spectroradiometer calibrated against a laser spectrum analyser (LSA) at the ns-OPO setup. As reference detector for the spectral irradiance responsivity measurements, a calibrated three-element trap detector equipped with a calibrated aperture was used.

The spectral responsivity of PFR-N-001 was measured over the wavelength range 300 nm to 1100 nm after accurate positioning and alignment of the instrument. Measurement overview is presented in figure 1.

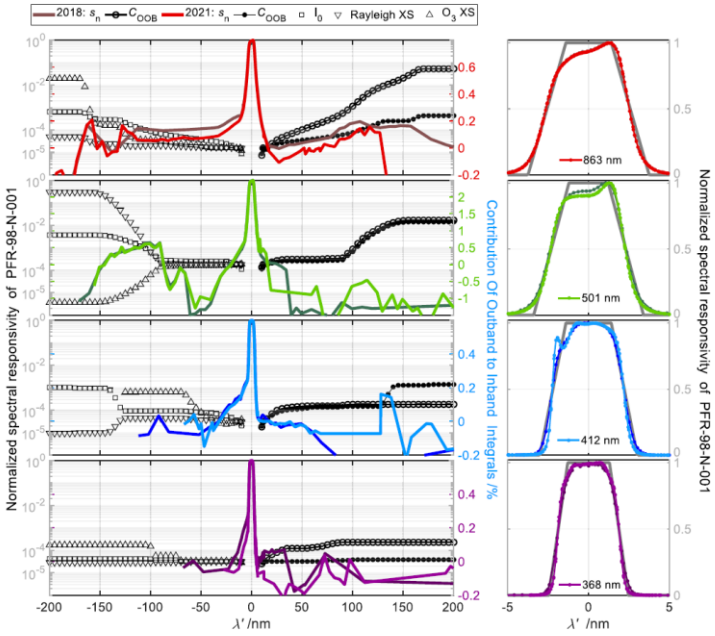

Fig. 1 Left panels: normalized spectral responsivity of the four channels of PFR-98-N-001 measured in 2018 (dark coloured lines) and 2021 (bright coloured lines) in logarithmic scale as a function of wavelength offset from the centroid wavelength λ. The contribution of the out-of-band to the in-band integral of the spectral responsivity, is shown for the two calibrations in % on the right axis (open circles: 2018, filled circles: 2021). Similarly, the contribution to the convolved TOA spectrum), and the ozone and Rayleigh cross

sections are plotted. Right panels: the spectral responsivity measured in 2018 and 2021 along with an approximated trapezoid filter function.

PFR top-of-the-atmosphere irradiance

TOA irradiance values provided by the above-mentioned published TOA solar irradiance spectra to those derived from the calibrated PFR measurements traceable to the SI using the Langley extrapolation technique. The high spectral resolution TOA solar spectra, were selected as follows:

• QASUMEFTS (Gröbner et al 2017): in this study it was used for the spectral range from 300 nm to 450 nm covering the 368 nm and 412 nm PFR channels;

• ATLAS-3 (Thuillier et al 2003, Chance and Kurucz 2010): it was used for the range 450 nm–1100 nm covering the 500 nm and 862 nm PFR channels.

• TSIS-1 HSRS (Coddington et al 2021): in the range 300 nm–1100 nm, covering all four PFR channels (ITSIS 0 (λ)).

The characterized at PTB PFR has measured in parallel with the WORCC triad at Davos. Three different AOD datasets has been produced and compared with the WORCC triad. Two of them using the PTB direct sun calibration traceable to SI each one of them using one of the above three mention TOA spectra (QASUMEFTS and ATLAS-3 were combined spectrally). The third one transferring the state of the art Langley calibration. Comparison results are presented in the publication highlight figure (2).

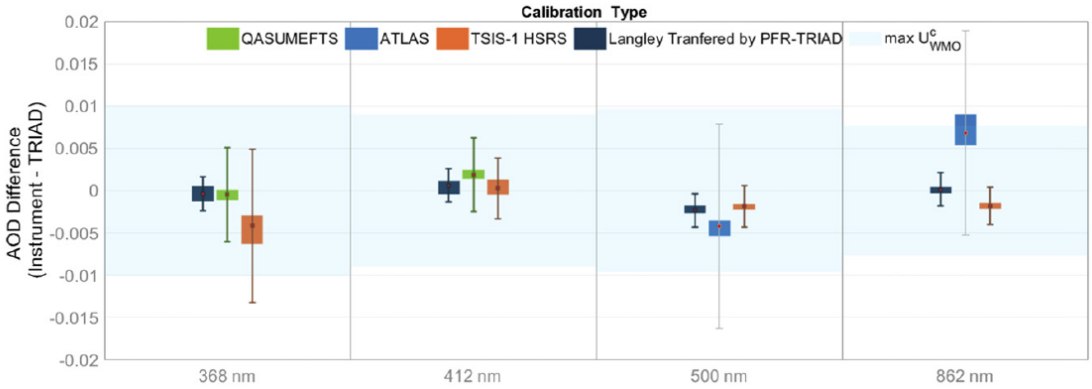

Fig. 2 Panels for the four PFR channels showing the median AOD differences of the 3 methods (Langley-based), (QASUMEFTS & ATLAS-3) and (TSIS-1 HSRS) to the PFR-TRIAD (red dots). The coloured squares represent the 5th and 95th percentile of the differences, while the error bars represent the expanded uncertainty U (k = 2) in the AOD from each method accounting for the uncertainty of the TOA spectrum and the PFR calibration.

Main outcomes: Calibration factors agreed within ±0.57% (3σ) using all three TOA spectra except for 368 nm (−1.1%) and 862 nm (1.8%) channels for one out of the three TOA spectra. Application of these results to the AOD retrieval showed AOD differences with the current reference methods/instruments well within the recommended WMO limits.

The main uncertainty for this new SI-based calibration method is the one related to the TOA spectrum used (either ground or space-based), compared with the laboratory-based calibration uncertainty of 0.3% (k = 2) or less.

This work aims at contributing towards an assessment of AOD uncertainties as an inherent requirement of traceable measurements, which is currently lacking in all main global aerosol monitoring networks. Results demonstrate the opportunity of cross-network implementation opportunities including a global AOD measurement harmonization and quality-controlled datasets, in line with the Harmonia objectives.

Based on the paper conclusions: "*The work provides a step of a new era of AOD measurements traceability, linked to the SI, through a laboratory-based approach, with the main advantages being the low uncertainty, the possibility of enhancing global AOD homogenization efforts and the chance to avoid calibration activities based on instrument relocations.*"

Spectral aerosol optical depth from SI-traceable spectral solar irradiance measurements

Based on the results of the MAPP project Gröbner et al., 2023 is dealing no more with filter-based AOD measurements, but with spectroradiometric ones. Spectroradiometric measurements of direct solar irradiance traceable to the SI were performed by three spectroradiometer systems during a 3-week campaign in September 2022 at the Izaña Atmospheric Observatory (IZO) located on the island of Tenerife, Canary Islands, Spain. The spectroradiometers provided direct spectral irradiance measurements in the spectral ranges:

- 300 to 550 nm (QASUME),
- 550 to 1700 nm (QASUME-IR),
- 300 to 2150 nm (BiTec Sensor, BTS), and
- 316 to 1030 nm (Precision Solar Spectroradiometer, PSR),

with relative standard uncertainties of 0.7 %, 0.9 %, and 1% for QASUME/QASUME-IR, the PSR, and the BTS respectively.

The calibration of QASUME and QASUME-IR was validated prior to this campaign at PTB. The ToA solar irradiance spectra from the spectroradiometers were retrieved from direct solar irradiance measurements using zero-air-mass extrapolation during cloud-free conditions, which were then compared to the TSIS-1 Hybrid Solar Reference Spectrum (HSRS). The comparison of ground-based-derived ToA and satellite/hybrid- based (TSIS) has been performed in order to understand differences and uncertainty sources on AOD calculations.

ToA solar spectra agreed to within 1% for spectral ranges higher than 400 nm (for QASUME also at shorter wavelengths) in spectral regions, free of significant trace gas absorption. They were within the combined uncertainties over the full investigated spectral range. By utilizing results from the QASUME vs TSIS comparison, the relative standard uncertainty of the TSIS-1 HSRS ToA solar spectrum (308 to 400 nm) is be reduced from its nominal 1.3% to 0.8 %.

Results presented as ratios of all spectroradiometers and one PFR instrument to the TSIS-1 HSRS are presented in figure 3.

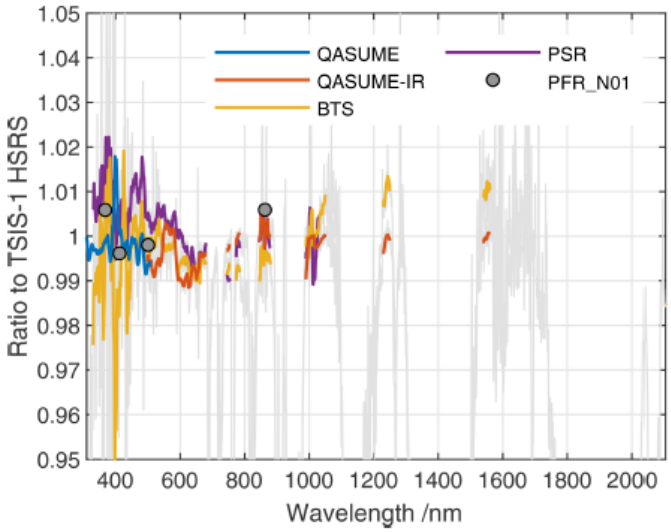

Fig. 3, Spectral ratio of the zero-air-mass-extrapolated ToA solar spectra from QASUME (blue), QASUME-IR (red), the PSR (violet), and the BTS (yellow) relative to the TSIS-1 HSRS convolved with the respective line spread functions of the spectroradiometers. The coloured lines are a 10 nm moving average of the spectral ratios in spectral regions with no or only weak atmospheric trace gas absorption, while the grey line represents the full spectral ratio of the BTS to the TSIS-1 HSRS. The grey circles represent the ratios of the spectral solar irradiances of PFR N01 with the TSIS-1 HSRS convolved with the spectral filter transmissions of PFR N01.

AODs have been calculated based on the above from all sun photometers available (CIMEL, PFR) and spectroradiometers mentioned above. Figure 4 shows the diurnal variation in the AOD at the common spectral channels of the sun photometers for this same day.

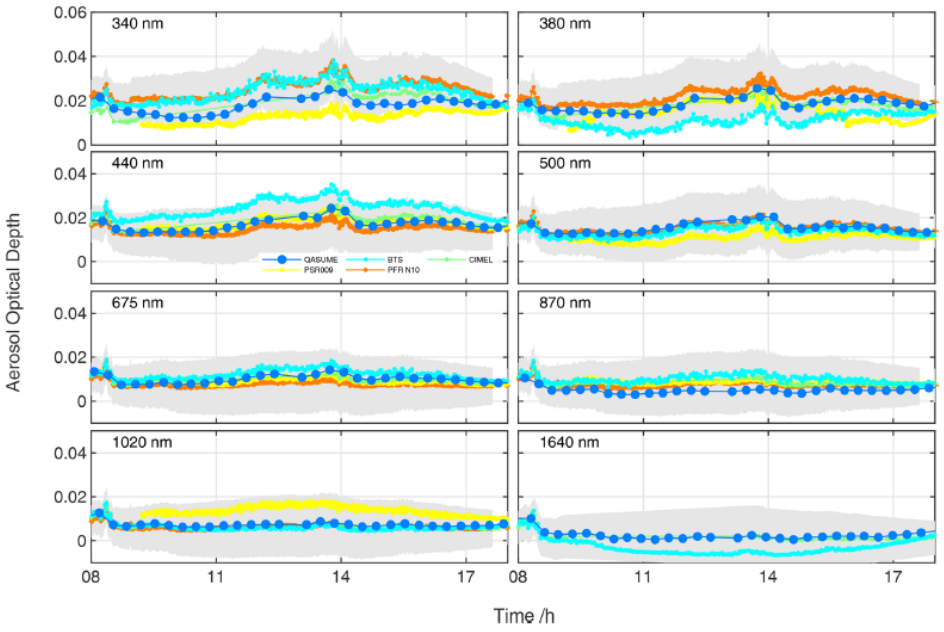

Fig. 4 Diurnal variation in the AOD on 13 September 2022 for the spectral channels of the Cimel sun photometer. The AOD from QASUME and QASUME-IR (blue dots), the BTS (light blue), and the PSR (yellow) are averaged over a 5 nm wide spectral band centred on the respective wavelength. The AODs from the PFR (orange) shown at 340, 380, and 440 nm were interpolated to the nearby spectral channels of the Cimel sun photometer (green) using the Ångström coefficients retrieved from its four spectral channels. The measurements of QASUME-IR and the BTS at nominally 1640 nm were obtained from averaging their measurements at 1560 nm to avoid the trace gas absorptions at 1640 nm. The grey area represents the WMO limit in which the measurements between different instruments are assumed equivalent.

Conclusions of the work of Gröbner et al: Global aerosol remote sensing networks (e.g. AERONET or GAW-PFR) rely on calibration techniques for network filter radiometers through outdoor comparisons with reference radiometers. However, traceability of such radiometers can be achieved through SI traceable sources. This can be achieved through regular calibrations of the reference radiometers in the metrological laboratories. An alternative could be the use of collocated reference PFR radiometers at different network calibration sites. This is the main philosophy planned for the Centre for Aerosol Remote sensing (CARS) of ACTRIS, which operates the European component of AERONET. At these three calibration sites, all

CARS–AERONET radiometers are calibrated with respect to the CARS master radiometers; PFR radiometers traceable to the SI would be operated simultaneously with the ACTRIS–AERONET master radiometers and would thereby extend the traceability to the whole CARS– AERONET network to SI traceable direct sun based AOD.

Sensitivity of global direct aerosol radiative forcing to uncertainties in aerosol optical properties

A third publication within the MAPP project was written by Elsey et al., 2023. The work approached direct effects of Aerosol properties related uncertainties to the calculation of global direct radiative forcing. The objective of the work is to try to apply different approaches on AOD uncertainty estimation to the actual effects on radiative forcing calculations. In a few words to assess the limitations of radiative forcing calculations based on existing Aerosol optical properties data accuracy.

There is an international effort of both the satellite and the ground based aerosol remote sensing measuring community to reduce the uncertainties of aerosol optical properties. It is still unclear how those reductions will propagate to uncertainties in the shortwave (SW) direct aerosol radiative effect (DARE) and radiative forcing (DARF), which are currently large, on the order of at least 20%.

Esley et al used a Monte-Carlo approach to calculate the impact of uncertainties in:

- aerosol optical depth (AOD),
- single scattering albedo (SSA) and
- asymmetry parameter

on the uncertainty of SW DARE and DARF. The approach used model outputs of over 2.3 million radiative transfer simulations to calculate global cloud free DARE and DARF. Different scenarios included different ranges of aerosol optical property uncertainties, representative of existing and future global observing systems.

A highlight figure of the paper presenting DARE sensitivity both at ToA and at the surface to the uncertainties to the above mentioned aerosol properties is shown below.

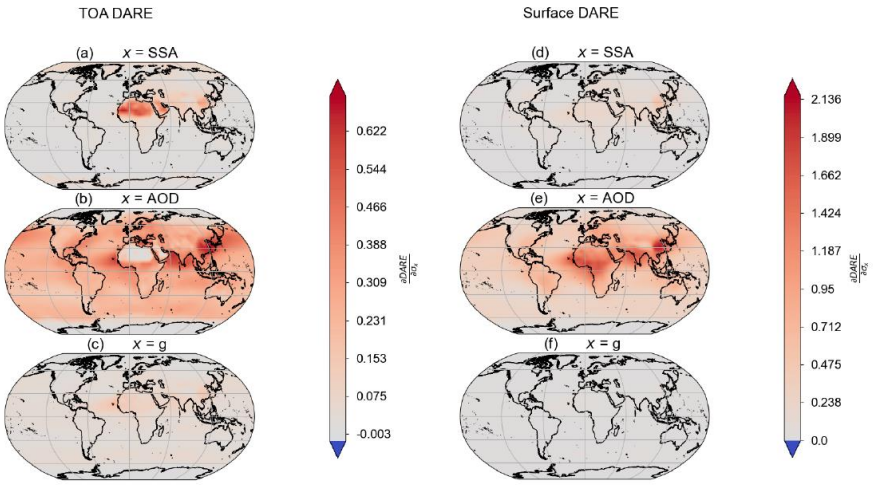

*Fig. 5. Sensitivity of Direct Aerosol Radiative Effect (DARE) at top-of-atmosphere (TOA) (left) and surface (right) to uncertainties in aerosol optical depth (AOD), single-scattering albedo (**ω0**) and asymmetry parameter (g). Units are W m-2 per unit optical property uncertainty.*

At the TOA, AOD uncertainty contributes the most to overall uncertainty, except over bright surfaces (e.g. desert areas) where SSA uncertainty contributes most. In addition, authors have applied regionally varying uncertainties to represent current measurement uncertainties, finding that aerosol optical property uncertainties represent 24% of TOA DARE and DARF.

Scaling these results to all-sky conditions, aerosol optical property uncertainty contributes to about 25% total uncertainty in TOA, all-sky DARE and DARF.

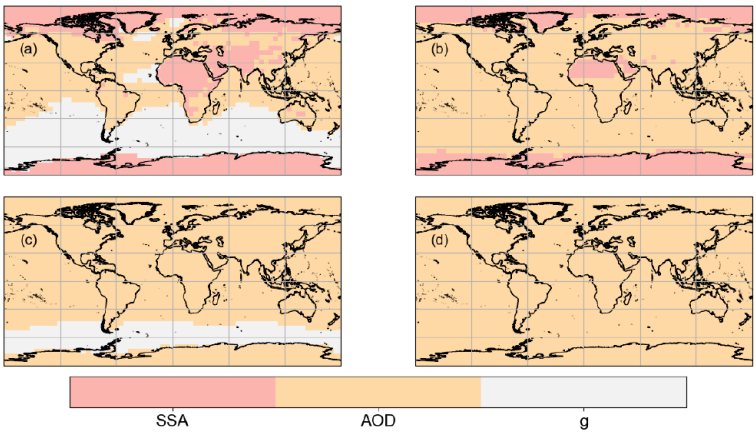

Fig. 6 The largest contributor to the uncertainty in each of the three single scattering properties for four different cases: top of atmosphere (TOA) Direct Aerosol Radiative

Forcing (DARF, panel (a)), TOA Direct Aerosol Radiative Effect (DARE, panel (b)), surface DARF (panel (c)) and surface DARE (panel (d)).

Main conclusions of the work: One-sigma uncertainty varies between ±0.23 to ±1.91 Wm-2 (5 and 42%) for the top of atmosphere (TOA) clear-sky DARE and between ±0.08 to ±0.47 Wm-2 (9 and 52%) for the TOA DARF. The implementation of the uncertainties were approached in two ways:

Assuming uniform uncertainties globally: "aerosol optical property uncertainties represent between 5 and 42% of DARE and 9 and 52% of DARF uncertainty at the TOA. At the TOA, AOD uncertainty is the main contributor to overall uncertainty, except over bright surfaces where SSA uncertainty contributes most."

Assuming regionally varying uncertainties: "aerosol optical property uncertainty contributes to about 25% uncertainty in TOA, all-sky DARE and DARF."

Discussing about effects of uncertainties from aerosol optical properties, clouds and surface reflectance, "aerosol optical property uncertainty accounts for a third to a half of total uncertainty". Suggesting that reducing the overall uncertainty, aerosol uncertainty reduction should be combined with reductions in non-aerosol uncertainties, such as surface and cloud properties.

Links with Harmonia

The MAPP project has contributed significantly to various aspects of aerosol remote sensing measurements and effects. Here we presented four relevant to Harmonia aspects.

a. A theoretical analysis of a detailed uncertainty estimation accompanies by the example of this estimation for the three largest sun photometric networks. This can be used by any aerosol measuring scientist (inside or outside Harmonia) as a start for calculating relevant instrument uncertainties. This summary is inline with both WG1 and 2 of Harmonia on measurement improvement and homogenization.
b. An introduction to a new era of calibration principles. Going from "artificial" reference sources and non-absolute calibrated measurements to Si traceable direct sun calibrations for filter radiometers. Including the method uncertainty. The work here is directly related with the global harmonisation aspects that WG2 of Harmonia is dealing.
c. A demonstration of the performance of instruments with larger potential on providing aerosol information (at least spectrally) with the analysis of spectroradiometric AOD retrieval. In addition, an assessment of the top of the

atmosphere spectra that are used (ground based, satellite based and hybrid) and their uncertainty contribution to AOD calculations. The work is online with WG 2 Harmonia objectives but also WG 4 towards using new technologies for AOD retrievals.

d. A study introducing the effects of uncertainties of different aerosol properties related with attenuation, absorption to scattering ratio and directional scattering preference to the calculation of SW radiation and aerosol direct radiative effects. The study is in line with the Harmonia WG3 objectives, and in particular with the community dealing with global radiative forcing assessment including aerosols.

References

Publications summarized:

Natalia Kouremeti, Saulius Nevas, Stelios Kazadzis, Julian Gröbner, Philipp Schneider and Kerstin Maria Schwind, SI-traceable solar irradiance measurements for aerosol optical depth retrieval, Metrologia, Volume 59, Number 4, https://doi.org/10.1088/1681-7575/ac6cbb, 2022

Gröbner, J., Kouremeti, N., Hülsen, G., Zuber, R., Ribnitzky, M., Nevas, S., Sperfeld, P., Schwind, K., Schneider, P., Kazadzis, S., Barreto, Á., Gardiner, T., Mottungan, K., Medland, D., and Coleman, M.: Spectral aerosol optical depth from SI-traceable spectral solar irradiance measurements, Atmos. Meas. Tech., 16, 4667–4680, https://doi.org/10.5194/amt-16-4667-2023, 2023

Elsey, J., Bellouin, N., and Ryder, C.: Sensitivity of global direct aerosol shortwave radiative forcing to uncertainties in aerosol optical properties, Atmos. Chem. Phys., 24, 4065–4081, https://doi.org/10.5194/acp-24-4065-2024, 2024.

other

Coddington O M, Richard E C, Harber D, Pilewskie P, Woods T N, Chance K, Liu X and Sun K 2021 The TSIS-1 hybrid solar reference spectrum Geophys. Res. Lett. 48 e2020GL091709

SchusterM, Nevas S, Sperling A and Völker S 2012 Spectral calibration of radiometric detectors using tunable laser sources Appl. Opt. 51 1950–61

Thuillier G, Hers´e M, Labs D, Foujols T, Peetermans W, Gillotay D, Simon P C and Mandel H 2003 The solar spectral irradiance from 200 to 2400 nm as measured by the SOLSPEC spectrometer from the Atlas and Eureca missions Sol. Phys. 214 1–22

Toledano C et al 2018 Assessment of sun photometer Langley calibration at the high-elevation Shaw G E 1983 Sun photometry Bull. Am. Meteor. Soc. 64 4–10

Gröbner, J., Kröger, I., Egli, L., Hülsen, G., Riechelmann, S., and Sperfeld, P.: The high-resolution extraterrestrial solar spectrum (QASUMEFTS) determined from ground-based solar irradiance measurements, Atmos. Meas. Tech., 10, 3375–3383, https://doi.org/10.5194/amt-10-3375-2017, 2017.

Cuevas, E., Romero-Campos, P. M., Kouremeti, N., Kazadzis, S., Räisänen, P., García, R. D., Barreto, A., Guirado-Fuentes, C., Ramos, R., Toledano, C., Almansa, F., and Gröbner, J.: Aerosol optical depth comparison between GAW-PFR and AERONET-Cimel radiometers from long-term (2005–2015) 1 min synchronous measurements, Atmos. Meas. Tech., 12, 4309–4337, https://doi.org/10.5194/amt-12-4309-2019, 2019

ANNEX 1

Uncertainty Budget for PFR-CIMEL-PREDE

The uncertainty components depend on the airmass and specific wavelength. For this table, the compiled values are calculated for a solar zenith angle of 60° (airmass 2), a wavelength of 500 nm and a pressure of 1013.15 mbar, O3=350 DU, NO2 =0.2 DU and AOD at 500 nm = 0.15 and Aer. radii 0.2 µm. Tables 1 (PFR), table 2 (CIMEL) and table 3 (Prede POM) are presented below including actual AOD components uncertainties and total uncertainty. The results have been provided as reported by the three calibration teams (CIMEL, PFR, Prede POM), participating in MAPP.

Table 1: Optical depth uncertainty budget for a reference precision filter radiometer (PFR) of GAWPFR-WORCC at 500 nm and at ground level for O3=350 DU ,N02 =0.2 DU and AOD at 500 nm = 0.15. The resulting optical depth uncertainty is unitless.

Parameter	Value xi	Uncertainty unit	Uncert type	Distribution	Nb. Deg. Freedom	Uncertainty u(xi)	Sensitivity coeff. C	C.u(xi)	Unit
I	2	Relative	A	Normal	10	5.77E-03	0.50	2.89E-	aod (dimensionless)
$I^{rel}_{FOV_{strl}}$	0	Relative				4.00E-04	0.50	2.00E-	
$I^{rel}_{Cleaning}$	0	Relative		Rectangula		5.00E-04	0.50	2.50E-	
I^{rel}_{Clouds}	0	Relative		Rectangula		0.00E+00	0.50	0.00E+0	
$I0$	3.7	Relative	A	Normal	30	1.40E-03	0.50	7.00E-	
P	1013.1	mbar	B	Normal		2.00E+00	7.1E-5	1.41E-4	
τ_{ray}	0.1434	OD				5.8E-04	1.00	5.8E-04	
$\tau N02$	0.001	OD	B	Rectangula		$u(TC_{NO2})$	1.00	2.49E-	
$\tau O3$	0.0118	OD	B	Rectangula		$u(TC_{O3})$	1.00	1.80E-	
M	2		B	Rectangula		5.77E-04	0.075	4.33E-	
m_{ray}	2		B	Rectangula		5.77E-04	0.072	4.14E-	

m_{O3}	2		B	Rectangula		1.70E-03	0.011	1.92E-	
m_{NO2}	2		B	Rectangula		5.77E-04	0.001	5.76E-	
XS_{ray}	0.1434	1/cm	B	Rectangula		5.90E-04	1.000	5.90E-	
XS_{o3}		1/DU	B	Rectangula		1.16E-03	0.350	4.07E-	
XS_{N02}		1/DU	B	Rectangula		4.96E-05	0.200	9.92E-	
Combined uncertainty								**0.0031**	
Expanded uncertainty (k=2)								**0.0063**	

Table 2 Uncertainty budget for a reference CE318 CIMEL radiometer from AERONET and at ground level for O3=350 DU ,N02 =0.2 DU and AOD at 500 nm = 0.15. The resulting optical depth uncertainty is unitless.

Parameter	Value xi	Uncertainty unit	Uncert type	Distribution	Nb. Deg. Freedom	Uncertainty u(xi)	Sensitivity coeff. C	C.u(xi)	Unit C.u(xi)
I	<2	Relative	A						Aod
dark		Relative	A	Normal		1E-6	0.5	5E-7	
OOB		Relative	A	Normal		0.0005	0.5	2.5E-4	
std		Relative	A	Normal		0.0006	0.5	0.0003	
T		Relative	A	Normal		0.00003	0.5	1.5E-5	
FOV	2	Relative	A	Normal		0.001	0.5	5E-4	
I0		Relative	A	Normal		0.001	0.5	5E-4	
P	1013.15	mbar	B	Rectangular		2			
τ_{ray}	0.1434	$u^2(XSray)+u^2(P)$				8.66E-6 , 5.77 E-4	1.00	5.8E-4	
τN02	0.001		B	Rectangular		2.88E-5	1.00	2.88E-5	
τO3	0.0118		B	Rectangular		0.0013	1.00	0.0013	
τH2O	PWV= 1 cm		B	Rectangular		0	1.00	0	
τgases			B	Rectangular		0	1.00	0	
M	2		B	Rectangular		5.77E-4	0.075	4.33E-5	
m_{ray}	2		B	Rectangular		5.77E-4	0.072	4.14E-5	
m_{O3}	2		B	Rectangular		1.70E-3	0.011	1.92E-5	
m_{NO2}	2		B	Rectangular		5.77E-4	0.001	5.76E-7	
XS_{ray}	0.5 nm	1/cm	B	Rectangular		5.90E-4	1.000	5.90E-4	

XS_{mo3}	0.5 nm	1/DU	B	Rectangular		1.16E-3	0.350	4.07E-4	
XS_{NO2}	0.5 nm	1/DU	B	Rectangular		4.96E-5	0.200	9.92E-6	
							Combined uncertainty	**0.002**	
							Expanded uncertainty (k=2)	**0.004**	

Table 3: Optical depth uncertainty budget for a Prede radiometer of SKYNET at 500 nm and at ground level for O3=350 DU, NO_2 =0.2 DU and AOD at 500 nm = 0.15. The resulting optical depth uncertainty is unitless.

Parameter	Value xi	Uncertainty unit	Uncert type	Distribution	Nb. Deg. Freedom	Uncertainty u(xi)	Sensitivity coeff. C	C.u(xi)
I		Relative	A	normal		0.0021	0.5	1.1E-3
$I^{rel}_{FOV_{strl}}$		Relative				0.0011	0.5	5.5E-4
$I^{rel}_{Cleaning}$		Relative				0.001	0.5	5.0E-4
I_0		Relative	A	normal		0.0087	0.5	4.4E-3
P	1013.25	mbar	B	rectangular		2		
τ_{Ray}	0.1434	OD				0.00060	1.0	6.0E-4
τ_{O3}	0.0118	OD	B	rectangular		0.00068	1.0	6.8E-4
τ_{NO2}	0.001	OD	B	rectangular		0.00029	1.0	2.9E-4
m	2		B	Rectangular		0.0024	0.075	1.8E-4
m_{ray}	2		B	Rectangular		0.00016	0.072	1.2E-5
m_{O3}	2		B	Rectangular		0.0032	0.011	3.5E-5
m_{NO2}	2		B	rectangular		0.0056	0.001	5.6E-6
XS_{Ray}		1/cm	B	Rectangular		5.90E-04	1.000	5.90E-04
XS_{O3}		1/DU	B	Rectangular		1.16E-03	0.350	4.07E-04
XS_{NO2}		1/DU	B	Rectangular		4.96E-05	0.200	9.92E-06
							Combined uncertainty	0.005
							Expanded uncertainty (k=2)	0.010

b. An Example of Machine learning on aerosol retrievals: Aerosol properties retrieval in partially cloud conditions using HDR All-Sky imagery

We present a new approach to determine aerosol properties from radiometrically calibrated images provided by an all-sky camera. It is designed to be used regardless of the sky conditions. However, we especially focus on partially cloudy scenes, which is the main novelty of this work.

We have used data from the instrumentation deployed in the Burjassot AtmoSpheric Station (BASS), which is maintained by the Solar Radiation Group of the University of Valencia (GRSV). BASS is a ground-based measurements station located in the eastern part of Spain (39.51 N, −0.42 W) within the metropolitan area of Valencia, 10 km away from the Mediterranean coast. The measurements are focused to monitor aerosols, clouds, solar and atmospheric radiation through remote sensing and in situ instruments.

The main instrument used in this work is an all-sky camera, SONA-201-D, which has been manufactured by Sieltec Canarias S.L. The SONA has a digital body color camera using a fisheye lens. All of this is encapsulated in a thermally controlled environment housing. The sensor mounts an RGB filter and an infrared blocking window, so the images have three channels with effective wavelengths of 615 ± 6 nm, 541 ± 5 nm and 480 ± 6 nm for red, green and blue, respectively (Valdelomar et al., 2021). The camera has been characterized and set to furnish geometrically and radiometrically calibrated high dynamic range (HDR) images of the sky, with 180◦ field of view. Therefore, we measure the radiance coming from every portion of the sky dome, with the spatial resolution defined by the camera observation geometry in terms of pixel zenith, azimuth, and solid angles.

The methodology starts with a three phase preprocessing of images and signals:

(A) crop-off the images: as first step we crop-off the images and only viewing zenith angles less than 75 degrees are used. This avoids the presence of buildings surrounding the station within the image.

(B) cloud identification: we have developed a methodology to build a useful input signal for our ML model, even when clouds fall within our region of interest in the image (Fig. 1(a)). Given an all-sky camera image, an approximation of the plane signal is derived by averaging the radiance in each isoline of scattering angle within the considered sector of the image (Fig. 1(a)). This principal plane proxy signal is composed by 35 radiance values related to a welldefined scattering angle. *This signal can be directly related to aerosol properties only in case that the whole sector is free of clouds, without the presence of glitters in the principal plane associated with the optics of our camera (Fig. 1b)* Keeping in mind that we want to solve the problem of clouds within our working scene in the image, we identify those scattering angles which are partially or totally cloudy from our previously averaged signal, and flag them (Fig. 1(b)).

(C) Generation of input signals: once the cloudy points are identified, we take advantage of Pérez model to reconstruct the RGB principal plane radiance at these cloudy points as if no clouds were present. The approach here is to use the radiance of the free-sky points of the signal to fit the principal plane Pérez formula and to obtain the radiance in the cloudy parts as if no clouds were there. The Perez formula represents the particularization of the Pérez model to the principal plane developed by Chauvin et al.

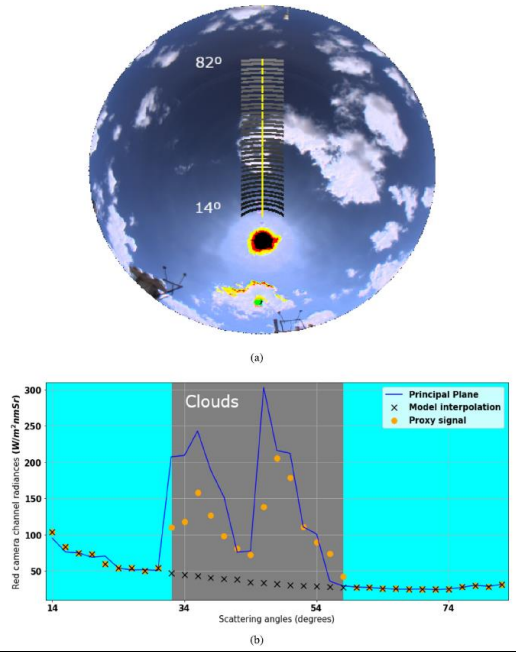

Figure 1. (a) All-sky camera image of a partially cloud scenario, including our working sector of the image and the isolines of scattering angles (in gray). (b) Principal plane radiance for the image in (a) (blue line); single scattering isoline averaged values (orange dots) lastly, our ML input signal (black crosses) obtained from the fit of the Perez model formula on free sky points (orange dots in the blue part of the graph).

A Gaussian Process Regressor (GPR) has been used as ML technique. An additional and interesting feature of the GPR is its ability to propagate the statistical

uncertainties based on the trained model. We use the standard deviation of these uncertainties to assess the quality of a single prediction. It is possible since the standard deviation of less accurate predictions is systematically larger than that corresponding to the accurate predictions. Therefore, we can consider quality assured predictions if their standard deviation does not exceed a certain threshold.

Results

We have applied our ML models to the 2-year dataset of the all-sky camera imagery, from 10th February 2020 to 31st March 2022. We have used from 72,314 to 74,404 images, depending on the channel, that fulfil the criteria needed to apply our ML models in the test phase. On average, the 87% of the images correspond to clear-sky conditions and the remaining 13% present partial cloudiness within our work sector in the image. Our ML models show a good overall performance in predicting aerosol optical properties (Table 1) both, the whole dataset and the quality assured data. Considering the whole dataset, for AOD the RMSE and MAE are in general slightly higher than the AERONET uncertainties for all the predicted variables. In addition, more than 80% of our predictions from the whole set fall within the 2x AERONET nominal uncertainties, whereas it is substantially reduced if we consider 1x AERONET nominal uncertainties. For AOD, RMSE and MAE significantly decrease with increasing wavelength, while by the contrary the number of our predictions within the AERONET uncertainties ($Nu1$ and $Nu2$) and the correlation coefficients increase. This suggests a better performance of our models for longer wavelength channels. The application of the quality criteria substantially improves our ML results in the comparison against AERONET from all points of view (values between brackets in Table 1). On the one hand, the proportion of predictions within the AERONET uncertainties significantly increases, showing $Nu1$ greater than 83% for AOD and 77% for AE. If we consider $Nu2$ a notably improvement is observed up to 96% in all predicted variables. It is especially noticeable in the prediction of AE. On the other hand, the MAE and RMSE values are well below the AERONET measurement uncertainties, with an outstanding maximum MAE (RMSE) of 0.006 (0.010) for AOD at 440 and a 0.05 (0.01) for AE. The spectral differences observed in the statistics for the AOD predictions are reduced radically when the quality assured data are used. It is clearly observed in MAE and RMSE, as well as in the correlation coefficients, which all exceed 0.97, and in the slopes of the comparison, which are

closer to unity for all the analyzed variables (Table 1). When we do not impose quality assured criteria, our general results show good agreement with AERONET, although greater variability is observed (blue dots in Fig. 3). On the contrary, the comparison is excellent when we only use quality assured data (colored data superimposed in Fig. 3, where color indicates the density of points). Most of our quality assured data falls within the uncertainty of AERONET measurements (black lines in Fig. 3), and moreover the data spread is dramatically reduced for all the variables analyzed. However, the strict quality control that we apply to our ML observations results in a significant reduction in the number of available observations. Thus, the proportion of data that meet our quality criteria represents 53%–60%of the initial data, depending on the channel (Table 1).

Table 1. Statistics of the predicted aerosol properties in comparison with AERONET data. Results for the quality assured predictions are within the brackets. N_{u1} and N_{u2} are the percentage of predictions that differ from AERONET data less than 1x and 2x the nominal AERONET uncertainty, respectively.

	MAE	$RMSE$	$Nu_1(\%)$	$Nu_2(\%)$	$SLOPE \pm \delta$	$INTERCEPT \pm \delta$	R^2
AOD_{675}	0.009 (0.004)	0.019 (0.007)	75 (90)	90 (99)	0.983 (0.996) ± 0.001	0.0016 (0.0004) ± 0.0001	0.92 (0.98)
AOD_{500}	0.012 (0.005)	0.025 (0.008)	69 (88)	85 (97)	0.994 (0.996) ± 0.001	0.0016 (0.0007) ± 0.0001	0.91 (0.98)
AOD_{440}	0.015 (0.006)	0.029 (0.010)	63 (83)	80 (96)	1.018 (0.999) ± 0.001	−0.0009 (0.0003) ± 0.0002	0.90 (0.98)
AE	0.11 (0.05)	0.17 (0.10)	63 (77)	84 (98)	1.003 (1.002) ± 0.002	−0.007 (0.001) ± 0.002	0.80 (0.97)

Our new approach is designed to be used also when clouds appear within our working sector in the image, and this is the main innovation of the present work. our method is stable and not very sensitive to external and methodological factors, especially when we apply quality assurance criteria.

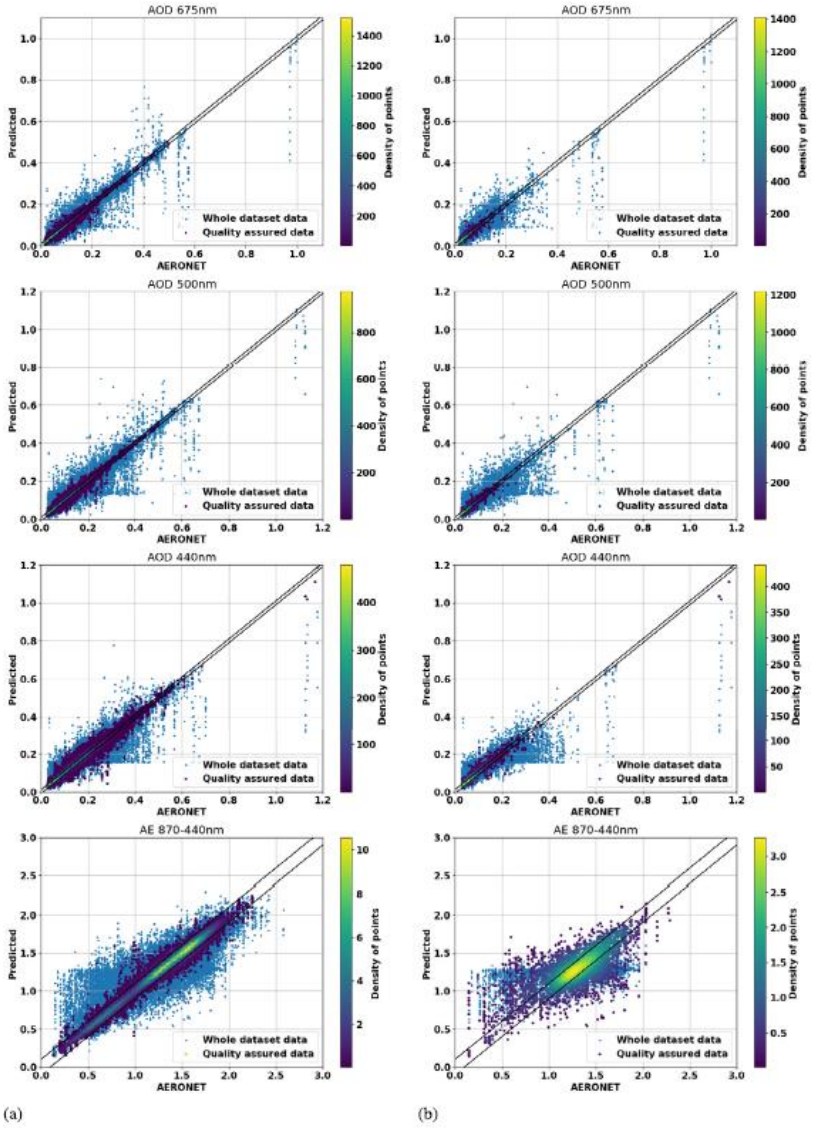

Figure 3. (a) Scatterplot of ML predictions vs AERONET aerosol properties. The black lines represent the nominal AERONET uncertainty limits in AOD and AE. (b) The same graphs of (a) are reported only for cases in which partially cloudy scenes are used.

References

- Scarlatti, F., et al., 2023. A machine learning approach to derive aerosol properties from all-sky camera imagery. Remote Sens. 15 (6), 1676. http://dx.doi.org/10.3390/rs15061676.
- Chauvin, R., et al., 2015. Modelling the clear-sky intensity distribution using a sky imager. Sol. Energy 119, 1–17. http://dx.doi.org/10.1016/j.solener.2015.06.026.

- Valdelomar, P., et al., 2021. Feasibility of ground-based sky-camera HDR imagery to determine solar irradiance and sky radiance over different geometries and sky conditions. Remote Sens. 13 (24), 5157. http://dx.doi.org/10.3390/rs13245157.